Development of La Doped Ni/CeO$_2$ for CH$_4$/CO$_2$ Reforming

Federica Menegazzo [1] , **Cristina Pizzolitto** [1], **Elena Ghedini** [1], **Alessandro Di Michele** [2] ,
Giuseppe Cruciani [3] **and Michela Signoretto** [1,*]

[1] CATMAT Lab, Department of Molecular Sciences and Nanosystems, Ca' Foscari University Venice and INSTM-RU Ve, Via Torino 155, 30172 Venezia Mestre, Italy; fmenegaz@unive.it (F.M.); cristina.pizzolitto@unive.it (C.P.); elena.ghedini@unive.it (E.G.)

[2] Department of Physics and Geology, University of Perugia, Via Pascoli, 06123 Perugia, Italy; alessandro.dimichele@unipg.it

[3] Department of Physics and Earth Science, University of Ferrara, Via Saragat 1, 44122 Ferrara, Italy; cru@unife.it

* Correspondence: miky@unive.it; Tel.: +39-041-234-8650

Abstract: Methane dry reforming (MDR) allows the transformation of carbon dioxide and methane, the two main greenhouse gases, into syngas. Given the high endothermicity of the process, it is necessary to produce a catalytic system that is very active, selective and resistant to coking deactivation; this work focuses on the development of a heterogeneous catalyst based on nickel supported on cerium oxide. Several strategies of synthesis of the catalysts were studied with particular attention to the lanthanum addition methodology. Both supports and catalysts, fresh and used, were deeply characterized by different techniques (N$_2$ physisorption, TPR, XRD, SEM). The effect of temperature on activity and selectivity of the different catalysts was also studied. A positive effect of lanthanum addition is strongly related to the synthetic methodology. Incipient wetness impregnation of lanthanum precursor on an already calcined ceria has led to the best catalytic activity. This behaviour is due to a more effective interaction between nickel and the support, which results in a higher dispersion of the active phase. The structural modifications have led to an improvement of the redox pump of the ceria, reducing the formation of coke during the reaction and improving the stability on time on stream.

Keywords: dry reforming; CO$_2$ reforming; Ni/CeO$_2$; lanthanum; La$_2$O$_3$; SMSI; ceria; syngas

1. Introduction

The greenhouse effect is a natural phenomenon caused by the presence of gases in the atmosphere and it allows an average temperature of the earth of 14 °C [1,2]. The main greenhouse gases are: water vapor, carbon dioxide, methane, ozone, nitrous oxide and some fluorinated gases (hydrofluorocarbons, sulphur hexafluoride, perfluorocarbons). Today it is known that the excessive presence of gas in the atmosphere alters the thermal equilibrium of the planet, causing climatic and environmental changes. The long period of persistence in the atmosphere of 50/200 years [3] and the high concentration, increased exponentially up to today's value (from 280 ppm before the industrial revolution to 406 ppm) [4], make carbon dioxide the main greenhouse gas. It has become, therefore, extremely important to keep the concentration of this gas under control [5,6]; a method widely used to reduce its emissions is known as CO$_2$ capture and storage (CCS) [7–9]. A more secure alternative to CCS is CO$_2$ capture and Utilization (CCU); the latter provides for the capture of CO$_2$, its purification and its use [10,11]. CCUs, compared to CCSs, have significant advantages [12] because they allow

transforming a waste gas such as CO_2 into chemical resources, solving both economical and sustainable issues. CO_2 can be directly used or converted into chemicals and fuels [13]. Although CO_2 is considered one of the most important greenhouse gases, methane, despite its lower concentration in the atmosphere, is believed to have a pollutant effect for global warming 24 times higher than CO_2 [14]. Methane can be reformed into syngas in the presence of an oxidizing agent and a proper catalytic system. The main method industrially used for the production of the syngas is the steam reforming of methane:

$$CH_4 + H_2O \leftrightarrows 3H_2 + CO \quad \Delta H^0 = +206 \text{ KJ/mol}$$

Other processes are the partial oxidation of methane:

$$CH_4 + \frac{1}{2}O_2 \leftrightarrows 2H_2 + CO \quad \Delta H^0 = -36 \text{ KJ/mol}$$

and methane dry reforming (MDR):

$$CH_4 + CO_2 \leftrightarrows 2H_2 + 2CO \quad \Delta H^0 = +247 \text{ KJ/mol}$$

With the modification of the oxidant, there is a variation of the reaction parameters including the kinetics, the endothermicity of the process and the H_2/CO ratio. The steam reforming of methane allows the highest ratio H_2/CO (which is 3), it is strongly endothermic and it is generally carried out at temperatures between 750 and 1450 °C and at pressures between 5 and 25 atm [15], in the presence of nickel-based catalysts supported on aluminium or magnesium oxides. On the contrary, the reaction of partial oxidation of methane is exothermic but has several problems connected to the formation of hot spots on catalytic systems, which entail their deactivation [16] and to the need for separation of oxygen from the air [17]. MDR uses CO_2 as an oxidant and synthesize a syngas with ratio 1 [18]. Despite the high endothermicity [19], MDR is a very promising process from the point of view of environmental impact [20,21]. In fact, from this reaction it is possible to consume two of the major greenhouse gases that are transformed into a chemical resource of significant industrial use. In order to make the process feasible, it is necessary to develop a catalytic system that allows the reaction to be carried out at relatively low temperatures and that is very active, selective and above all resistant to coking deactivation. In fact, there are many reactions involved in the MDR process [22], such as the Reverse Water Gas Shift:

$$CO_2 + H_2 \leftrightarrows H_2O + CO \quad \Delta H^0 = +41 \text{ KJ/mol}$$

which is favoured at high temperatures and involves the consumption of H_2 with the formation of CO, so this reaction can vary the final H_2/CO ratio. The MDR process is complicated by further reforming reactions [23]:

$$CH_4 + H_2O \leftrightarrows 3H_2 + CO \quad \Delta H^0 = +206 \text{ KJ/mol}$$

$$CH_4 + 2H_2O \leftrightarrows 4H_2 + CO_2 \quad \Delta H^0 = +165 \text{ KJ/mol}$$

These too can result in a change in the final H_2/CO ratio. Moreover, during the process there are different reactions, which lead to the formation of carbon and depend on reaction temperature. For example, the decomposition of methane, that it is favoured by high temperatures and low pressures:

$$CH_4 \leftrightarrows C + 2H_2 \quad \Delta H^0 = +75 \text{ KJ/mol}$$

On the other hand, the disproportional reaction of the CO occurs at low temperature and at high pressure:

$$2CO \leftrightarrows C + CO_2 \quad \Delta H^0 = -172 \text{ KJ/mol}$$

In MDR process, therefore, coke is formed at both high and low temperatures and its presence is inevitable, mainly in the temperature range between 560 and 700 °C [24]. It is possible to decrease coke formation by modifying the gases ratio; for example, by introducing more CO_2, it is possible to move the balance of the CO disproportion to the left [25].

Other reactions that can form coke, both favoured at low temperatures, are the following:

$$CO_2 + 2H_2 \leftrightarrows C + 2H_2O \quad \Delta H^0 = -90 \text{ KJ/mol}$$

$$CO + H_2 \leftrightarrows C + H_2O \quad \Delta H^0 = -131 \text{ KJ/mol}$$

For MDR to have industrial validity it is necessary to develop a very active catalytic system that allows the reaction to take place even at low temperatures; at the same time, however, the catalyst must be very selective towards the products so as to limit the production of coke [26]. which, as seen, can be formed at both high and low temperatures.

In the literature, the catalytic systems initially studied used as active phase noble metals such as Rh, Ru, Pd and Pt [27–30] which, for MDR, have a high stability and activity and a good resistance to coke. However, these metals are not industrially convenient because they are very expensive [31]. A more economical alternative to noble metals is the use of transition metals such as Ni and Co. These latter have a lower activity compared to noble metals and consequently it is necessary to introduce them into the catalytic system in higher amounts. Ni is a very active metal in the splitting of the C–O and C–H bonds present in CO_2 and CH_4, respectively and is therefore suitable for the MDR process [32–47]. However, this element is not very stable at high temperatures and tends to sinter, which is a phenomenon strongly connected to coke formation [48]. For these reasons it is necessary to use an adequate support that has a high surface area and high porosity in order to allow a good dispersion of the active phase, making it more stable [49]. At the same time, it is important to obtain a catalytic system that is very selective towards the desired products and that reduces coke formation. The latter can be limited through the gasification of the coke ($C + CO_2 \leftrightarrows 2CO$) [50]. With the aid of basic promoters, it is possible to increase the absorption of CO_2, which is acid and therefore becomes more active for the reaction. In order to favour this type of mechanism, various supports have been studied such as MgO [51] and La_2O_3 [52], which being basic oxides facilitate the absorption of CO_2 on the support.

To reduce the formation of coke, supports with high oxygen mobility can also be used [53]; this is released during the reaction and, interacting with the carbonaceous species adsorbed on the catalyst, the oxide releases the active phase. An example of a support that has high oxygen mobility is the ceria, which acts as a redox cycle because it allows reversibly changing the oxidation state of the cerium from 4+ to 3+ [54], releasing oxygen according to the reaction:

$$2CeO_2 \leftrightarrows Ce_2O_3 + \frac{1}{2}O_2$$
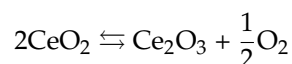
In this way, the holes are generated on the support and the oxygen that is released can oxidize the carbonaceous compounds in CO and CO_2, prolonging the life of the catalytic system. Moreover, ceria redox cycle is involved in the mechanism of methane dry reforming. Laosiripojana et al. demonstrated that CeO_2 reacts with CH_4 producing CO and H_2, leaving CeO_{2-n} ($CeO_2 + nCH_4 \rightarrow CeO_{2-n} + nCO + 2nH_2$). The reduced form of CeO_2 reacts then with CO_2 producing CO and restoring its original form ($CeO_{2-n} + nCO_2 = CeO_2 + nCO$) as proposed by Mars van Krevelen mechanism [55,56]. The ceria, despite these excellent properties, is not very stable at high temperatures; for this reason, it requires promoters to improve its thermal resistance. An interesting compound that can be used to improve the properties of ceria support is lanthanum. It could improve the thermal stability of the support and at the same time increase the oxygen vacancies, modifying ceria redox and structural properties [56,57]. Moreover, as mentioned above, it is possible that lanthanum oxide, being basic, improves the absorption of CO_2 and its interaction with the catalyst. Lanthanum and cerium

oxide are generally used as promoters of different resistant supports such as ZrO_2 and Al_2O_3 [58–60]; according to our knowledges, only few existing works in literature introduce La_2O_3 as promoter for CeO_2 support. Pino et al. reported the effect of different La_2O_3 percentage on Ni/CeO_2 catalyst for methane tri-reforming process [61], meanwhile, the Authors reported the effect of La_2O_3 over Ni/CeO_2 catalyst for ethanol steam reforming [62]. In this work the attention has been focused on the synthetic methodologies of promoter introduction because it is an important parameter to investigate, allowing to modify the morphological-structural characteristics of the material and consequently its catalytic activity. The aim of this work is to develop Ni-based catalysts that are active, selective and stable in MDR. In particular, catalytic systems will be studied that use ceria as support; promoted with lanthanum oxide by three different methods, namely:

- Dry impregnation of the lanthanum precursor on the not calcined support of ceria;
- Dry impregnation of the lanthanum precursor on the calcined support of ceria;
- Co-precipitation of lanthanum and cerium precursors.

The goal is to evaluate the effect of lanthanum addition on the catalytic activity, in particular by studying the redox pump modifications determined by the addition of the precursor, the different metal support interaction and the dispersion of the active phase.

2. Materials and Methods

2.1. Catalysts Synthesis

Cerium support was synthesized by precipitation from $(NH_4)_2Ce(NO_3)_6$ (Aldrich, Italy) by urea at 100 °C in aqueous solution [56,63]. The solution was mixed at 100 °C for 6 h, the precipitate was washed, dried at 110 °C for 20 h (iCe). Part of the material was calcined at 550 °C (oCe).

Lanthanum (6% by weight) was added onto the support by three different ways:

- incipient wetness impregnation of $La(NO_2)_3 \cdot 6H_2O$ aqueous solution on iCe and calcination at 550 °C (iLaCe);
- incipient wetness impregnation of $La(NO_2)_3 \cdot 6H_2O$ aqueous solution on oCe and calcination at 550 °C (oLaCe);
- Co-precipitation of $(NH_4)_2Ce(NO_3)_6$ and $La(NO_2)_3 \cdot 6H_2O$ and calcination at 550 °C (cLaCe).

The metal introduction on the support was performed by incipient wetness impregnation with a proper amount of $Ni(NO_3)_2$ aqueous solution in order to obtain 8 wt % of nickel on the material. After drying at 110 °C for 15 h, a calcination was performed in flowing air (30 mL/min) at 550 °C for 3 h. The samples will be referred to as reported in Table 1.

Table 1. Samples' labels.

Methodology	Support	Sample
precipitation of Ce	Ce	Ni/Ce
impregnation of La on iCe	iLaCe	iNi/LaCe
impregnation of La on oCe	oLaCe	oNi/LaCe
co-precipitation of La and Ce	cLaCe	cNi/LaCe

2.2. Characterization Techniques

The Ni amount was determined by atomic absorption spectroscopy (AAS) after microwave disintegration of the samples (100 mg) using a Perkin-Elmer Analyst 100 (Perkin-Elmer, Waltham, MA, USA).

Surface areas and pore size distributions were obtained from N_2 adsorption/desorption isotherms at −196 °C using a Micromeritics ASAP 2000 analyser (Micromeritics, Norcross, GA, USA). Surface

area was calculated from the N_2 adsorption isotherm by the BET equation and pore size distribution was determined by the BJH method [64]. Total pore volume was taken at $p/p^0 = 0.99$.

TPR measurements were carried out in a lab-made equipment: samples (100 mg) were heated with a temperature rate of 10 °C/min from 25 °C to 900 °C in a 5% H_2/He flow (40 mL/min). The effluent gases were analysed by a TCD detector and by a Genesys 422 quadrupole mass analyser (QMS, ESS Ltd., Rotherham, UK).

X-ray powder diffraction (XRD) patterns were measured by a Bruker D8 Advance diffractometer (Bruker, Karlsruhe, Germany) equipped with a Si(Li) solid state detector (SOL-X) and a sealed tube providing Cu Kα radiation. The Rietveld refinement method as implemented in the Bruker TOPAS programme was used to obtain the refined unit cell parameters, crystal size and the quantitative phase analysis for the supports and metal phases in the samples. The crystal size determination is achieved by the integral breadth based calculation of volume weighted mean crystallize sizes.

FE-SEM images have been obtained using a Field Emission Gun Electron Scanning Microscopy LEO 1525 (Carl Zeiss Microscopy, Jena, Germany), after metallization with Chromium. The images were acquired by AsB (angular selective BSE) detector (Carl Zeiss Microscopy) while elemental composition was determined using Bruker Quantax EDS (Bruker Nano GmbH, Berlin, Germany).

2.3. Catalytic Tests

The catalytic tests were performed with a reference reactor PID (Process Integral Development Eng & Tech, Madrid, Spain) coupled to a gas-chromatograph (HP 6890) and to a Genesys 422 quadrupole mass analyser (QMS). A schematization is shown in Scheme 1. Microactivity-Effi is an automatic computerized high-pressure reactor, in which the whole system is kept heated inside a hot box (red square in Scheme 1). An automatic bypass valve allows to avoid the passage to the reactor of the reaction mixture, leading to the possibility to perform preliminary stability test of the mixture before the reaction. All tests can be programmed thanks to the use of the computer shown in the image. Reforming reaction was carried out with a total flow of 200 mL/min STP of 5% CH_4 and 5% CO_2 diluted in helium. The reaction temperature was between 400–550 °C. Preliminary blank tests, which consists in charging the reactor with only SiC and not catalyst, showed the absence of conversion at these temperatures.
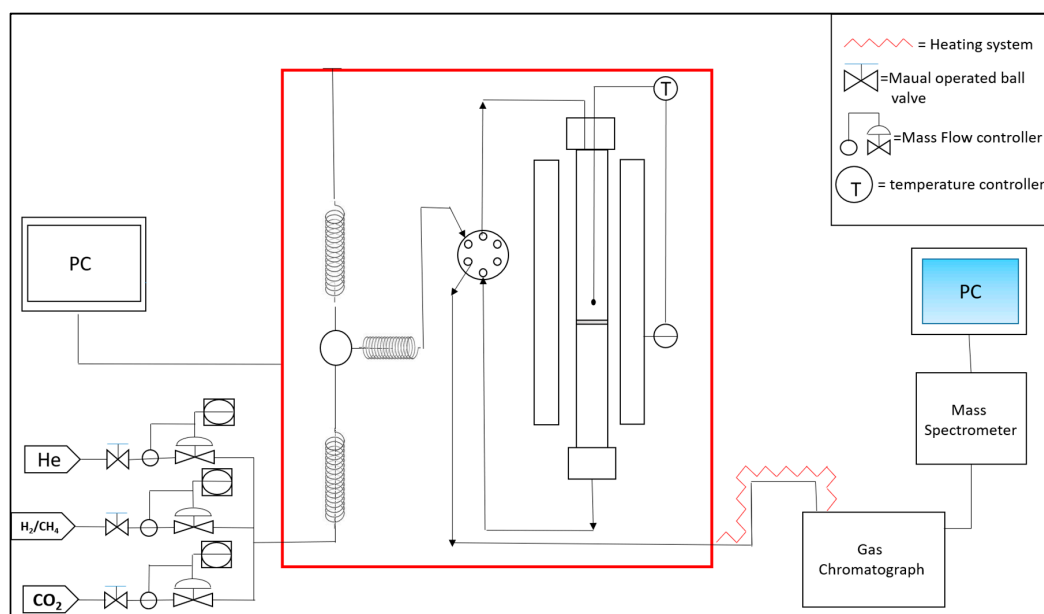
Scheme 1. Lab set-up.

The catalyst, after calcination, is pelletized and reduced into small pellets with an average size of 0.3–0.4 mm. The reactor is loaded with 150 mg of catalyst mixed with SiC. The sample reduction is performed in situ at 550 °C in H_2 with a flow of 30 mL/min for 1 h. After the analysis, the following data were calculated:

$$CH_4 \text{Conversion } (\%) = \frac{fCH_{4in} - fCH_{4out}}{fCH_{4in}} \cdot 100$$

$$CO_2 \text{Conversion } (\%) = \frac{fCO_{2in} - fCO_{2out}}{fCO_{2in}} \cdot 100$$

$$H_2 \text{Yield } (\%) = \frac{fH_{2out}}{2 \cdot fCH_{4in}} \cdot 100$$

$$CO \text{ Yield } (\%) = \frac{fCO_{out}}{fCH_{4in} + fCO_{2in}} \cdot 100$$

$$H_2/CO = \frac{fH_{2out}}{fCO_{out}}$$

$$\text{Carbon Balance } (\%) = \frac{fCH_{4out} + fCO_{2out} + fCO_{out}}{fCH_{4in} + fCO_{2in}} \cdot 100$$

3. Results and Discussion

Preliminary characterizations were carried out to determine some characteristics of the samples, such as the actual nickel content in the catalyst, the surface area and the reduction temperature of the active phase. Specifically, atomic absorption techniques, physisorption of N_2 and reduction in programmed temperature (TPR) were used respectively. Table 2 reports the effective amounts of nickel, which is almost the same for all samples (around 8 wt %).

The isotherms of the supports compared with those of the corresponding catalysts are shown in Figure 1. All curves are ascribable, according to the IUPAC classification, to type IV isotherms with a hysteresis loop characteristic of mesoporous materials. For all the samples, a decrease of surface area is observed passing from the support to the catalyst and this is due to the presence of the active phase (Table 2). The difference in surface area is more remarkable for the samples oNi/LaCe and cNi/LaCe. In particular, for the latter catalyst, a flattening and a translation of the hysteresis to lower pressure values is also observed, indicating the presence of smaller pores.

Table 2. Physicochemical properties of the Ni samples (Nickel amount calculated via Atomic Adsorption, Surface area via BET equation and Average pore diameter via BJH equation).

Sample	wt% Ni	m²/g	nm
Ce		107 (±1)	6.0
Ni/Ce	7.8 (±0.5)	82 (±1)	6.1
iLaCe		97 (±1)	6.2
iNi/LaCe	7.9 (±0.5)	71 (±1)	6.5
oLaCe		110 (±1)	5.8
oNi/LaCe	7.8 (±0.5)	66 (±1)	4.7
cLaCe		128 (±1)	5.1
cNi/LaCe	7.7 (±0.5)	77 (±1)	4.7

Figure 2 reports TPR profiles of the catalysts. For all samples, peaks between 160 and 420 °C are observed due to the reduction of Ni^{2+} to Ni^0. It is known that Ni is reduced from the 2+ state to 0 in a single stage; therefore, the presence of more peaks of reduction is due to the different interaction of Ni with the support. The peaks at lower temperatures are due to Ni species more easily reducible and therefore mildly interacting with the support [65]. On the contrary, the peaks at higher temperatures are due to Ni species that, interacting more strongly with the support, are more difficult to reduce. From this graph, it is possible to observe that the reduction profiles relative to the Ni/Ce, iNi/LaCe

and cNi/LaCe samples do not show significant differences in the 160–400 °C temperature range; in the case of the oNi/LaCe catalyst, on the other hand, a shift at higher temperatures can be observed for both peaks. This data highlights how in this sample there is a higher interaction between support and active phase. Moreover, it is possible to observe that nickel is reduced in any case below 400 °C; the reduction of the samples was then performed at 500 °C to be sure that all the nickel was present in the metallic form, active for the reaction, which was then conducted between 400 and 550 °C.
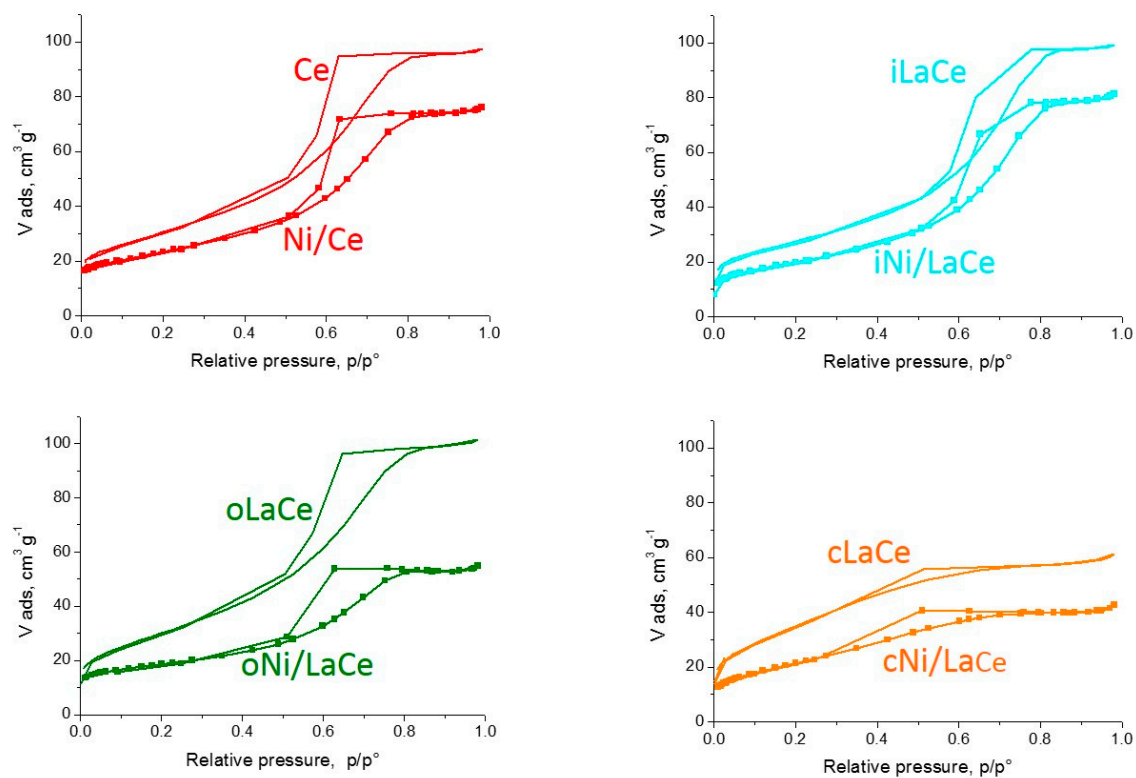
Figure 1. N_2 physisorption isotherms of the supports and the corresponding catalysts.
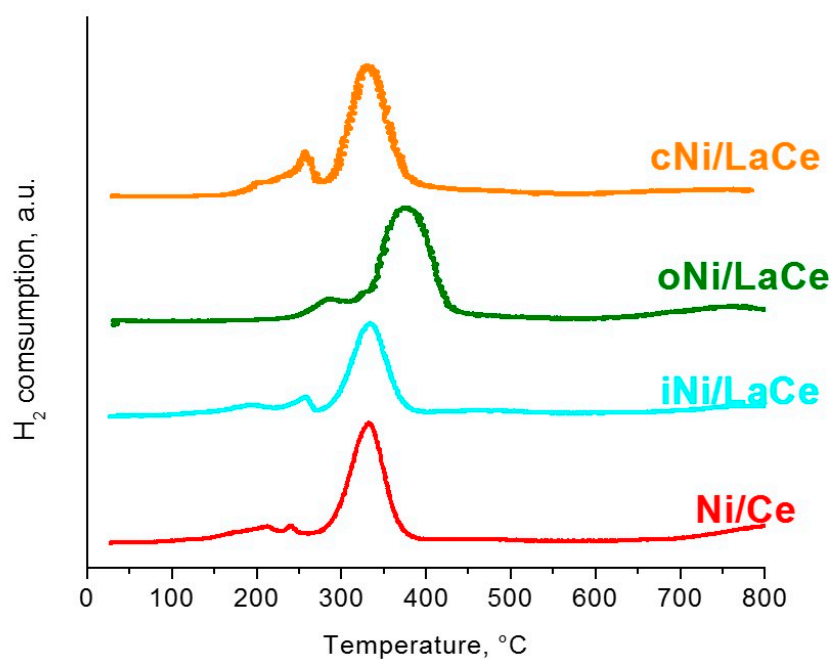
Figure 2. TPR patterns of the catalysts.

As previously stated, the MDR process is strongly endothermic and requires a considerable amount of energy. However, from an industrial point of view, it could be interesting to reduce as much as possible the temperature. In fact, syngas could be used for the synthesis of long chain hydrocarbons or oxygenate chemicals such as acetic acid, dimethyl ether and oxo-alcohols [66,67], which work at much lower temperature than a classic reforming. Therefore, we have first performed a temperature screening to understand whether the catalytic systems prepared in this work can be active at temperatures between 400 and 550 °C. Figure 3 reports data of H_2 yields (section a) and H_2/CO ratio (section b) for non-promoted Ni/Ce sample after 10 h of reaction. As it can be seen, as the reaction temperature increases, there is an increase in the H_2 yield, as expected for the endothermicity of the MDR process, even if the catalyst is active also at low temperature. The effect of temperature is observed not only in the activity of the catalyst but also in its selectivity. The ratio H_2/CO is always different from one, which is the stoichiometric ratio for MDR. Considering the lowest temperature (400 °C), the H_2/CO value is higher than one, while for higher temperatures it is always less than unity. It is hypothesized that these values are strongly influenced by the reaction of Water Gas Shift (WGS); this is exothermic and favoured at low temperatures. At 400 °C it allows a higher formation of H_2 and lower CO, resulting in a H_2/CO ratio higher than the unit. At higher temperatures this reaction is not very favoured and consequently the H_2/CO ratio is lowered. From literature data it has been observed that ceria based supports favour WGS at low temperatures, between 400–450 °C, above which the reaction is almost absent [68]. This can therefore justify a higher H_2/CO ratio which is only obtained at 400 °C. All samples promoted with lanthanum behaved similarly to Ni/Ce with the temperature as for H_2 yield and H_2/CO ratio.
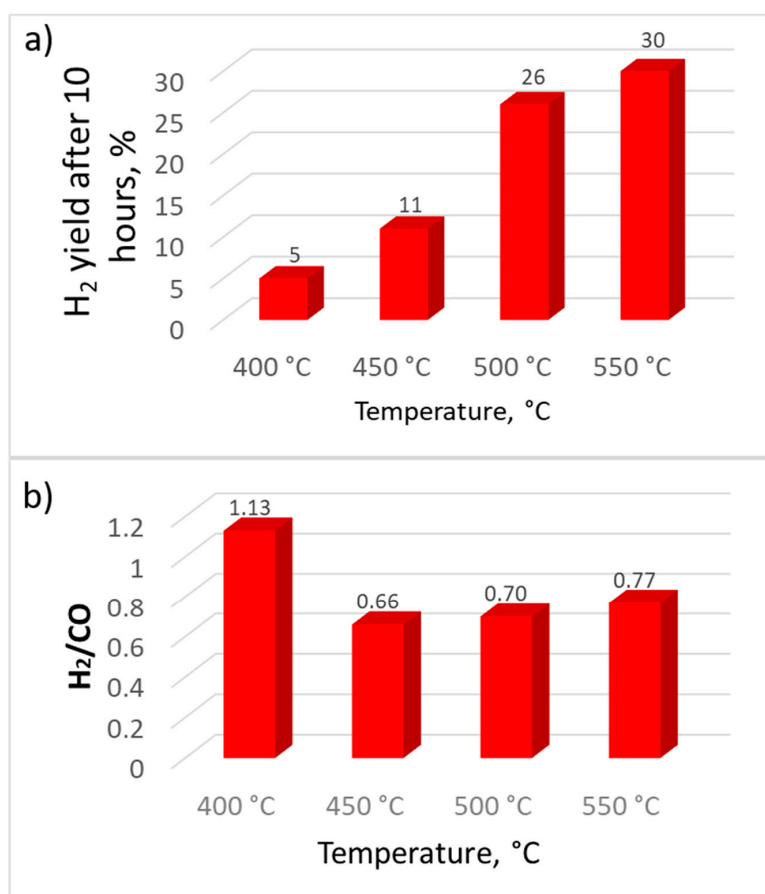

Figure 3. H_2 yield (**a**) and H_2/CO ratio after 10 h of reaction (**b**) for Ni/Ce catalyst at different temperatures.

In order to evaluate the effect of the introduction of lanthanum, the comparison between H_2 yields after 18 h of reaction at 550 °C for the different catalysts is reported in Figure 4. It is observed that all the promoted samples have a hydrogen yield higher than the Ni/Ce sample. This behaviour is even more pronounced for the sample prepared by impregnation of lanthanum on calcined cerium (oNi/LaCe). In terms of selectivity (as it is visible in Figure 3), however, no differences are observed with respect to the non-promoted sample. In fact, all the samples have the same trend over time for the H_2/CO ratio, which is comparable to that of Ni/Ce.
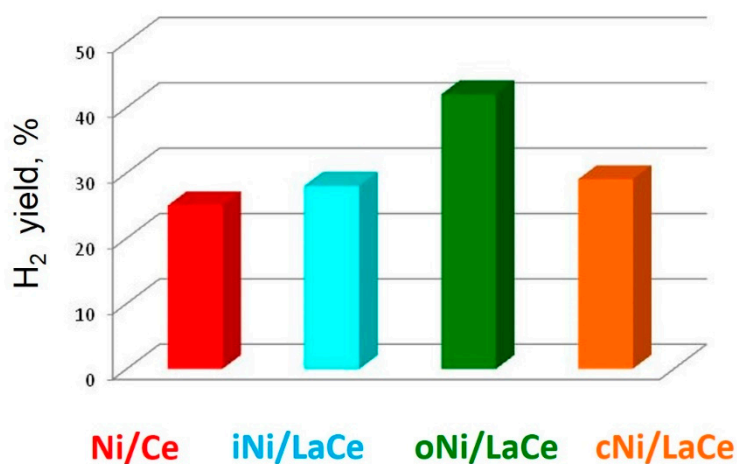
Figure 4. H_2 yield of the different samples after 18 h of reaction at 550 °C.

As assumed in the introduction, lanthanum is expected to influence the redox properties of ceria. To verify this hypothesis, TPR measurements were performed on the plain supports, in order to determine reducibility of all the systems (Figure 5).
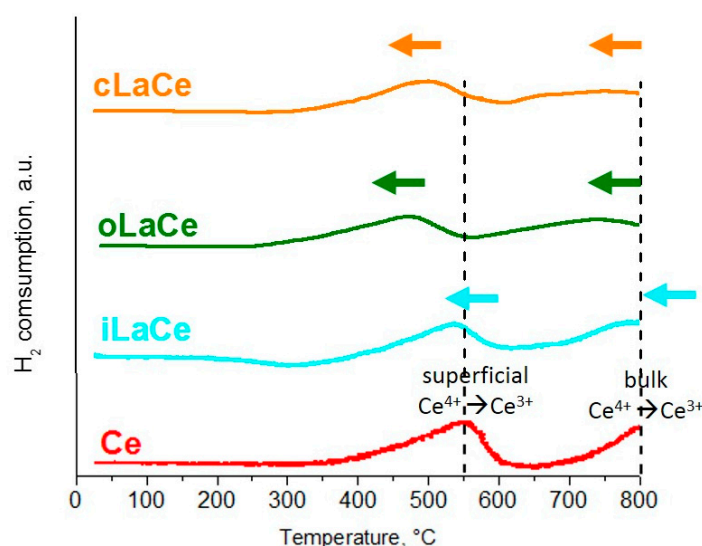

Figure 5. TPR profiles for the plain supports.

By evaluating the TPR profile of plain non promoted Ce, it is possible to observe two reduction peaks: the first one is between 400 and 600 °C, the second one above 680 °C. Both are attributable to the reduction of Ce^{4+} to Ce^{3+}: the first is related to the reduction of Ce^{4+} on the surface, the second one to the reduction of Ce^{4+} in bulk [69]. Considering the other profiles, we observe the presence of the same peaks, also due to the reduction of superficial and bulk Ce^{4+} to Ce^{3+}. In these curves, however, it is observed that the peaks are shifted to lower temperatures than those of the unpromoted ceria.

The shift of the peaks denotes a higher reducibility of the supports, in particular oLaCe and cLaCe, that could be due to the improvement of the redox cycle capacity, related to the introduction of lanthanum.

In order to better understand the role of lanthanum on the different catalytic systems, X-ray diffraction measurements have been carried out to evaluate the structure of the samples. Before the analysis, the catalysts were reduced and passivated at 500 °C in order to get as much closer to reaction conditions as possible. The catalysts have a fluorite type structure for the ceria [70–72] and nickel in its metallic form [73]. Very accurate cell parameter for ceria were determined by Rietveld profile fitting of the XRD (XRD spectra are reported in Figure S1 in Supplementary Material) patterns: an increase in this parameter was observed due to the introduction of lanthanum, as shown in Figure 6.
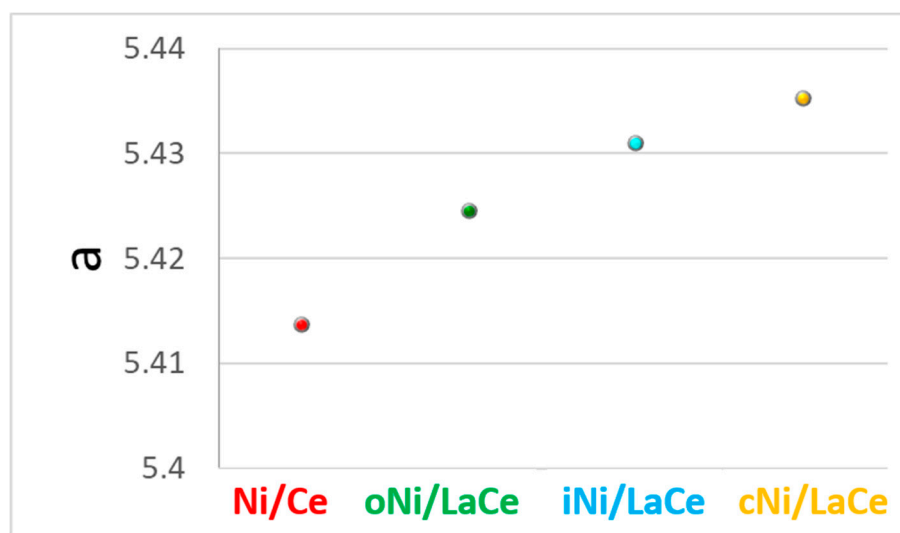

Figure 6. Variation of cell parameter of the catalysts obtained by Rietveld fit of XRD patterns.

It was observed that all the samples promoted with lanthanum show an increase in the cell parameter with respect to Ni/Ce. The presence of lanthanum on the support, independently of the synthetic methodology, causes a modification of the cell parameter. The increase in the cell parameter is more remarkable in the sample prepared by co-precipitation. It is hypothesized that the La^{3+} (11.6 nm ionic radius), replacing the Ce^{4+} ion (9.7 nm ionic radius), changes the oxygen stoichiometry of the ceria fluorite-type structure, improving its the redox cycle capacity. Indeed, literature data confirm that it is possible to replace 2 Ce^{4+} with 2 La^{3+}, which creates an oxygen gap on the ceria [74]. However, even if the effect of the redox cycle capacity is supposed to improve the catalytic behaviour, this modification does not fully justify the activity data, which therefore seems to be connected to other parameters as well. Through the Rietveld analyses, the particle size of the active phase was also determined (Table 3).

Table 3. Ni nanosize as determined by Rietveld method.

Sample	Ni Size, nm
Ni/Ce	18 (±1)
iNi/LaCe	16 (±1)
oNi/LaCe	11 (±1)
cNi/LaCe	15 (±1)

All La promoted samples have a smaller size than La-free Ni/Ce catalyst. In particular, the sample oNi/LaCe has smaller particles than all the other samples. Therefore, it appears that the best performance of this catalyst is related to the most effective dispersion of nickel, which is reflected in the smaller particle size [75]. This can be connected to the stronger metal support interactions, as revealed by TPR analyses previously discussed.

In Figure 7, the Carbon Balance trends of the best promoted sample and of the non-promoted one are reported. The promoted sample has higher values, indicating that the presence of lanthanum has allowed a lower formation of carbon compounds. In fact, the latter presents a carbon balance of almost 100%.
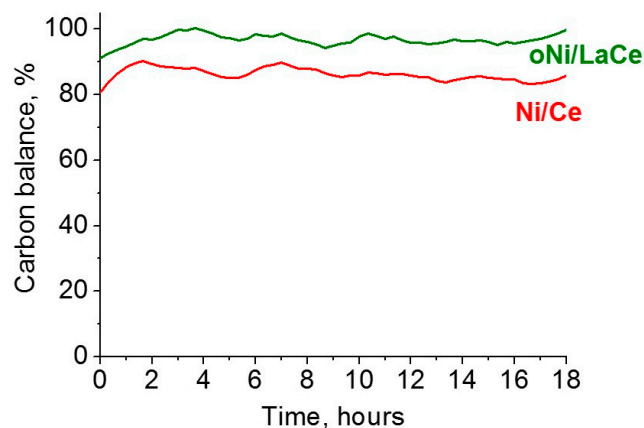

Figure 7. Carbon balance vs time of reaction at 550 °C for Ni/Ce and oNi/LaCe samples.

In order to confirm this hypothesis, we have carried out SEM and EDX measurements on the samples discharged after 18 h of reaction at 550 °C (Figure 8). From the SEM analyses, it has been observed that the Ni/Ce sample is more covered with coke, which is present in the form of nanotubes, than the promoted oNi/LaCe. These data seem to confirm the hypothesis that the presence of lanthanum and consequently the increase of the redox cycle capacity of the ceria, favour the removal of the carbonaceous species deposited on the surface of the catalyst, thus improving carbon balance.
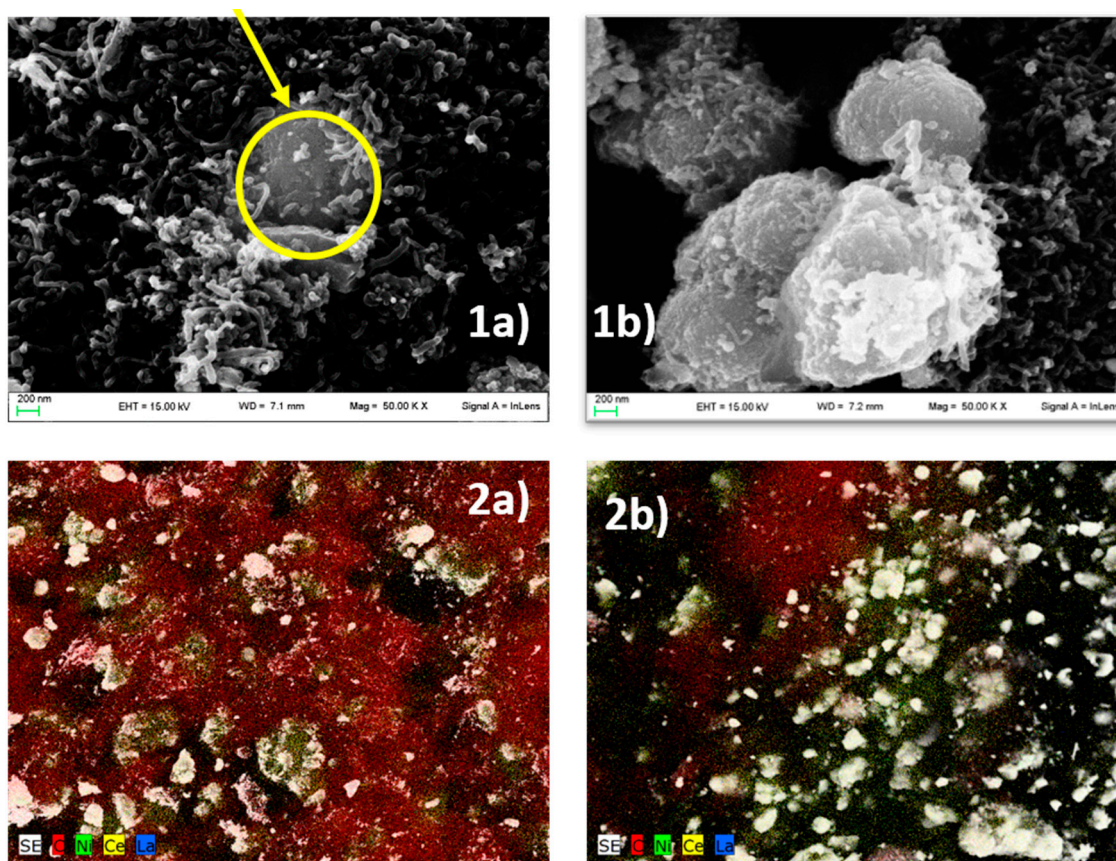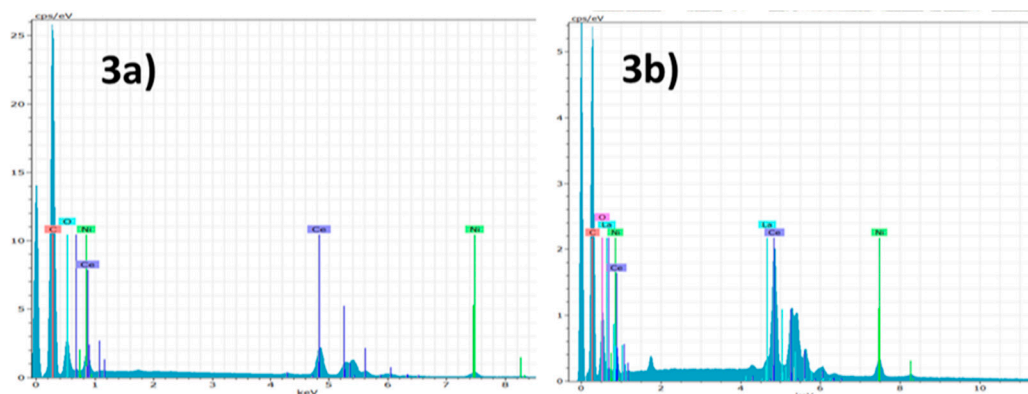

Figure 8. *Cont.*

Figure 8. SEM and EDX analyses for Ni/Ce (**1a**,**2a**,**3a**) and oNi/LaCe (**1b**,**2b**,**3b**).

Therefore, from the analyses carried out on these samples it can be observed how the synthesis methodology influences the activity of the catalytic system. The sample prepared by the introduction of lanthanum on calcined cerium (oNi/LaCe) presents the best catalytic behaviour. This is probably due to the more effective dispersion of the active phase favoured by a higher interaction of the nickel particles with the support and at the same time, by the increase of the redox cycle capacity of the support itself. To further investigate the catalytic behaviour of these two samples and in particular, to evaluate their stability over time, they were tested at 550 °C for 45 h. In Figure 9, the H_2 yields of the two catalysts are compared.
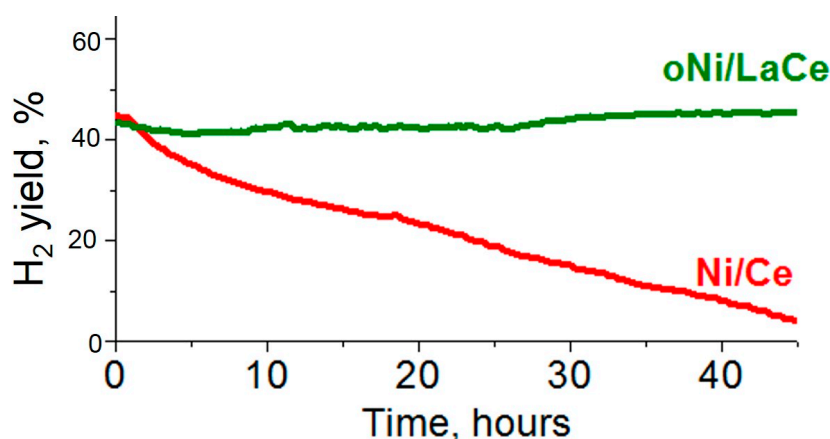

Figure 9. H_2 yield for reaction at 550 °C for Ni/Ce and oNi/LaCe samples.

As previously noted, the sample promoted with lanthanum (oNi/LaCe) has a higher production of hydrogen compared to the Ni/Ce sample. In this case, however, its stability over time is confirmed too. In comparison to Ni/Ce, which is almost completely deactivated after 45 h, the activity of oNi/LaCe is preserved, maintaining a constant hydrogen yield for a long time.

4. Conclusions

Lanthanum promotion of Ni based sample supported on ceria is effective for MDR. However, such positive effect is strongly related to the synthetic methodology. All the samples present higher activity and stability than the non-promoted ones; this higher stability is connected with the increment of ceria redox ability due to the introduction of lanthanum oxide. Partial substitution of Ce^{4+} with La^{3+} inside ceria lattice, demonstrated by XRD analyses, has brought to the increase of the electronic vacations of the support, leading to a higher reducibility of this, as it is visible by the TPR. These structural modifications have led to an improvement of the redox cycle capacity of the ceria, reducing the formation of coke during the reaction and improving the stability on time on stream. Nevertheless,

incipient wetness impregnation of lanthanum precursor on an already calcined ceria has led to the best catalytic activity. This behaviour is due to a more effective interaction between nickel and support, which results in a higher dispersion of the active phase. In fact, in this case, nickel presents lower dimension than other samples. Moreover, this catalyst has been tested for 42 h and it has presented stable hydrogen production for all the time of steam.

References

1. Lacis, A.A.; Schmidt, G.A.; Rind, D.; Ruedy, R.A. Atmospheric CO_2: Principal control knob governing Earth's temperature. *Science* **2010**, *330*, 356–359. [CrossRef] [PubMed]

2. Anderson, T.R.; Hawkins, E.; Jones, P.D. CO_2, the greenhouse effect and global warming: From the pioneering work of Arrhenius and Callendar to today's Earth System Models. *Endeavour* **2016**, *40*, 178–187. [CrossRef] [PubMed]

3. Tuckett, R.P. The Role of Atmospheric Gases in Global Warming Observed. In *Impacts on Planet Earth Elsevier*, 1st ed.; T.M. Letcher: Amsterdam, The Netherlands, 2009; pp. 3–19. ISBN 978-0-444-53301-2.

4. Intergovernmental Panel on Climate Change. *Climate Change 2014: Synthesis Report*; Intergovernmental Panel on Climate Change: Geneva, Switzerland, 2014; Available online: http://www.ipcc.ch/ (accessed on 27 September 2018).

5. United Nations Framework Convention on Climate Change (UNFCCC). *Adoption of the Paris Agreement*; Report No. FCCC/CP/2015/L.9/Rev.1; UNFCCC: New York City, NY, USA, 2015; Available online: http://unfccc.int/resource/docs/2015/cop21/eng/l09r01.pdf (accessed on 27 September 2018).

6. Rogelj, J.; den elzen, M.; Höhne, N.; Fransen, T.; Fekete, H.; Winkler, H.; Schaeffer, R.; Sha, F.; Riahi, K.; Meinshausen, M. Paris Agreement climate proposals need a boost to keep warming well below 2 °C. *Nature* **2016**, *534*, 631–639. [CrossRef] [PubMed]

7. Suzuki, T.; Toriumi, M.; Sakemi, T.; Masui, N.; Yano, S.; Fujita, H.; Furukawa, H. Conceptual Design of CO_2 Transportation System for CCS. *Energy Procedia* **2013**, *37*, 2989–2996. [CrossRef]

8. Onyebuchi, V.E.; Kolios, A.; Hanak, D.P.; Biliyok, C.; Manovic, V. A systematic review of key challenges of CO_2 transport via pipelines. *Renew. Sustain. Energy Rev.* **2018**, *81*, 2563–2583. [CrossRef]

9. Bruhn, T.; Naims, H.; Olfe-Kräutlein, B. Separating the debate on CO_2 utilisation from carbon capture and storage. *Environ. Sci. Policy* **2016**, *60*, 38–43. [CrossRef]

10. International Energy Agency (IEA). *Energy Technology Perspectives 2017*; IEA: Paris, France, 2017; Available online: http://www.iea.org/etp/ (accessed on 27 September 2018).

11. Centi, G.; Perathoner, S. Opportunities and prospects in the chemical recycling of carbon dioxide to fuels. *Catal. Today* **2009**, *148*, 191–205. [CrossRef]

12. Cuéllar-Franca, R.M.; Azapagic, A. Carbon capture, storage and utilisation technologies: A critical analysis and comparison of their life cycle environmental impacts. *J. CO2 Util.* **2015**, *9*, 82–102. [CrossRef]

13. Alper, E.; Orhan, O.Y. CO_2 utilization: Developments in conversion processes. *Petroleum* **2017**, *3*, 109–126. [CrossRef]

14. Yang, L.; Lu, F.; Zhou, X.; Wang, X.; Duan, X.; Sun, B. Progress in the studies on the greenhouse gas emissions from reservoirs. *Acta Ecol. Sin.* **2014**, *34*, 204–212. [CrossRef]

15. LeValley, T.L.; Richard, A.R.; Fan, M. The progress in water gas shift and steam reforming hydrogen production technologies—A review. *Int. J. Hydrog. Energy* **2014**, *39*, 16983–17000. [CrossRef]

16. Enger, B.C.; Lodeng, R.; Holmen, A. A review of catalytic partial oxidation of methane to synthesis gas with emphasis on reaction mechanisms over transition metal catalysts. *Appl. Catal. A Gen.* **2008**, *346*, 1–27. [CrossRef]

17. Abdullah, B.; Ghani, N.A.A.; Vo, D.N. Recent advances in dry reforming of methane over Ni-based catalysts. *J. Clean. Prod.* **2017**, *162*, 170–185. [CrossRef]

18. Wu, H.; Pantaleo, G.; La Parola, V.; Venezia, A.M.; Collard, X.; Aprile, C.; Liotta, L.F. Bi- and trimetallic Ni catalysts over Al$_2$O$_3$ and Al$_2$O$_3$-MO$_x$ (M = Ce or Mg) oxides for methane dry reforming: Au and Pt additive effects. *Appl. Catal. B Environ.* **2014**, *156–157*, 350–361. [CrossRef]

19. Bobrova, L.N.; Bobin, A.S.; Mezentseva, N.V.; Sadykov, V.A.; Thybaut, J.W.; Marin, G.B. Kinetic assessment of dry reforming of methane on Pt + Ni containing composite of fluorite-like structure. *Appl. Catal. B Environ.* **2016**, *182*, 513–524. [CrossRef]

20. Yu, M.; Zhu, K.; Liu, Z.; Xiao, H.; Deng, W.; Zhou, X. Carbon dioxide reforming of methane over promoted Ni$_x$Mg$_{1−x}$O (1 1 1) platelet catalyst derived from solvothermal synthesis. *Appl. Catal. B Environ.* **2014**, *148–149*, 177–190. [CrossRef]

21. Yu, M.; Zhu, Y.A.; Lu, Y.; Tong, G.; Zhu, K.; Zhou, X. The promoting role of Ag in Ni-CeO$_2$ catalyzed CH$_4$-CO$_2$ dry reforming reaction. *Appl. Catal. B Environ.* **2015**, *165*, 43–56. [CrossRef]

22. Wolfbeisser, A.; Sopriprun, O.; Bernardi, J.; Wittayakun, J.; Föttinger, K.; Rupprechter, G. Methane dry reforming over ceria-zirconia supported Ni catalysts. *Catal. Today* **2016**, *277*, 234–245. [CrossRef]

23. Nikoo, M.K.; Amin, N.A.S. Thermodynamic analysis of carbon dioxide reforming of methane in view of solid carbon formation. *Fuel Process. Technol.* **2011**, *92*, 678–691. [CrossRef]

24. Arora, S.; Prasad, R. An overview on dry reforming of methane: Strategies to reduce carbonaceous deactivation of catalysts. *RSC Adv.* **2016**, *6*, 108668. [CrossRef]

25. Alenazey, F.S. Utilizing carbon dioxide as a regenerative agent in methane dry reforming to improve hydrogen production and catalyst activity and longevity. *Int. J. Hydrog. Energy* **2014**, *39*, 18632–18641. [CrossRef]

26. Muraza, O.; Galadima, A. A review on coke management during dry reforming of methane. *Int. J. Energy Res.* **2015**, *39*, 1196–1216. [CrossRef]

27. Bitter, J.H.; Seshan, K.; Lercher, J.A. The State of Zirconia Supported Platinum Catalysts for CO$_2$/CH$_4$ Reforming. *J. Catal.* **1997**, *171*, 279–286. [CrossRef]

28. Bitter, J.H.; Seshan, K.; Lercher, J.A. On the contribution of X-ray absorption spectroscopy to explore structure and activity relations of Pt/ZrO$_2$ catalysts for CO$_2$/CH$_4$ reforming. *Top. Catal.* **2000**, *10*, 295–305. [CrossRef]

29. Nagaoka, K.; Seshan, K.; Lercher, J.A.; Aika, K. Activation mechanism of methane-derived coke (CH$_x$) by CO$_2$ during dry reforming of methane-comparison for Pt/Al$_2$O$_3$ and Pt/ZrO$_2$. *Catal. Lett.* **2000**, *70*, 109–116. [CrossRef]

30. Nagaoka, K.; Seshan, K.; Lercher, J.A.; Aika, K. Mechanism of carbon deposit/removal in methane dry reforming on supported metal catalysts. *Stud. Surf. Sci. Catal.* **2001**, *136*, 129–136.

31. Karemore, A.L.; Vaidya, P.D.; Sinha, R.; Chugh, P. On the dry and mixed reforming of methane over Ni/Al$_2$O$_3$—Influence of reaction variables on syngas production. *Int. J. Hydrog. Energy* **2016**, *41*, 22963–22975. [CrossRef]

32. Črnivec, I.G.O.; Djinović, P.; Erjavec, B.; Pintar, A. Effect of synthesis parameters on morphology and activity of bimetallic catalysts in CO$_2$-CH$_4$ reforming. *Chem. Eng. J.* **2012**, *207–208*, 299–307. [CrossRef]

33. Xu, L.; Song, H.; Chou, L. Carbon dioxide reforming of methane over ordered mesoporous NiO–MgO–Al$_2$O$_3$ composite oxides. *Appl. Catal. B* **2011**, *108–109*, 177–190. [CrossRef]

34. Min, J.E.; Lee, Y.J.; Park, H.G.; Zhang, C.; Jun, K.W. Carbon dioxide reforming of methane on Ni–MgO–Al$_2$O$_3$ catalysts prepared by sol–gel method: Effects of Mg/Al ratios. *J. Ind. Eng. Chem.* **2015**, *26*, 375–383. [CrossRef]

35. Rahemi, N.; Haghighi, M.; BaBaluo, A.A.; Jafari, M.F.; Estifaee, P. Synthesis and physicochemical characterizations of Ni/Al$_2$O$_3$–ZrO$_2$ nanocatalyst prepared via impregnation method and treated with non-thermal plasma for CO$_2$ reforming of CH$_4$. *J. Ind. Eng. Chem.* **2013**, *19*, 1566–1576. [CrossRef]

36. Jang, W.J.; Kim, H.M.; Shim, J.O.; Yoo, S.Y.; Jeon, K.W.; Na, H.S.; Lee, Y.L.; Jeong, D.W.; Bae, J.W.; Nah, I.W.; et al. Key properties of Ni–MgO–CeO$_2$, Ni–MgO–ZrO$_2$, and Ni–MgO–Ce(1 − x)Zr(x)O$_2$ catalysts for the reforming of methane with carbon dioxide. *Green Chem.* **2018**, *20*, 1621–1633. [CrossRef]

37. Roh, H.S.; Jun, K.W.; Dong, W.S.; Chang, J.S.; Park, S.E.; Joe, Y.I. Highly active and stable Ni/Ce–ZrO$_2$ catalyst for H$_2$ production from methane. *J. Mol. Catal. A Chem.* **2002**, *181*, 137–142. [CrossRef]

38. Valentini, A.; Carreno, N.L.V.; Probst, L.F.D.; Lisboa-Filho, P.N.; Schreiner, W.H.; Leite, E.R.; Lingo, E. Role of vanadium in Ni:Al$_2$O$_3$ catalysts for carbon dioxide reforming of methane. *Appl. Catal. A Gen.* **2003**, *255*, 211–220. [CrossRef]

39. Li, H.; Wang, J. Study on CO$_2$ reforming of methane to syngas over Al$_2$O$_3$–ZrO$_2$ supported Ni catalysts prepared via a direct sol–gel process. *Chem. Eng. Sci.* **2004**, *59*, 4861–4867. [CrossRef]

40. Juan-Juan, J.; Roman-Martinez, M.C.; Illan-Gomez, M.J. Effect of potassium content in the activity of K-promoted Ni/Al$_2$O$_3$ catalysts for the dry reforming of methan. *Appl. Catal. A Gen.* **2006**, *301*, 9–15. [CrossRef]

41. Luna, A.E.C.; Iriarte, M.E. Carbon dioxide reforming of methane over a metal modified Ni-Al$_2$O$_3$ catalyst. *Appl. Catal. A Gen.* **2008**, *343*, 10–15. [CrossRef]

42. Yamazaki, O.; Tomishige, K.; Fujimoto, K. Development of highly stable nickel catalyst for methane-steam reaction under low steam to carbon ratio. *Appl. Catal. A Gen.* **1996**, *136*, 49–56. [CrossRef]

43. Tomishige, K.; Kanazawa, S.; Sato, M.; Ikushima, K.; Kunimori, K. Catalyst Design of Pt-Modified Ni/Al$_2$O$_3$ Catalyst with Flat Temperature Profile in Methane Reforming with CO$_2$ and O$_2$. *Catal. Lett.* **2002**, *84*, 69–74. [CrossRef]

44. Nurunnabi, M.; Li, B.; Kunimori, K.; Suzuki, K.; Fujimoto, K.I.; Tomishige, K. Performance of NiO–MgO solid solution-supported Pt catalysts in oxidative steam reforming of methane. *Appl. Catal. A Gen.* **2005**, *292*, 272–280. [CrossRef]

45. Jeong, D.W.; Jang, W.J.; Shim, J.O.; Roh, H.S.; Son, I.H.; Lee, S.J. The effect of preparation method on the catalytic performance over superior MgO-promoted Ni–Ce$_{0.8}$Zr$_{0.2}$O$_2$ catalyst for CO$_2$ reforming of CH$_4$. *Int. J. Hydrog. Energy* **2013**, *38*, 13649–13654. [CrossRef]

46. Moradi, G.; Khezeli, F.; Hemmati, H. Syngas production with dry reforming of methane over Ni/ZSM-5 catalysts. *J. Nat. Gas Sci. Eng.* **2016**, *33*, 657–665. [CrossRef]

47. Xu, L.; Song, H.; Chou, L. One-Pot Synthesis of Ordered Mesoporous NiO–CaO–Al$_2$O$_3$ Composite Oxides for Catalyzing CO$_2$ Reforming of CH$_4$. *ACS Catal.* **2012**, *2*, 1331–1342. [CrossRef]

48. Song, J.H.; Han, S.J.; Yoo, J.; Park, S.; Kim, D.H.; Song, I.K. Hydrogen production by steam reforming of ethanol over Ni–X/Al$_2$O$_3$–ZrO$_2$ (X = Mg, Ca, Sr, and Ba) xerogel catalysts: Effect of alkaline earth metal addition. *J. Mol. Catal. A* **2016**, *415*, 151–159. [CrossRef]

49. Aramouni, N.A.K.; Touma, J.G.; Tarboush, B.A.; Zeaiter, J.; Ahmad, M.N. Catalyst design for dry reforming of methane: Analysis review. *Renew. Sustain. Energy Rev.* **2018**, *82*, 2570–2585. [CrossRef]

50. Zhang, L.; Zhang, Q.; Liu, Y.; Zhang, Y. Dry reforming of methane over Ni/MgO–Al$_2$O$_3$ catalysts prepared by two-step hydrothermal method. *Appl. Surf. Sci.* **2016**, *389*, 25–33. [CrossRef]

51. Wang, Y.; Liu, H.; Xu, B. Durable Ni/MgO catalysts for CO$_2$ reforming of methane: Activity and metal–support interaction. *J. Mol. Catal. A Chem.* **2009**, *299*, 44–52. [CrossRef]

52. Li, X.; Li, D.; Tian, H.; Zeng, L.; Zhao, Z.; Gong, J. Dry reforming of methane over Ni/La$_2$O$_3$ nanorod catalysts with stabilized Ni nanoparticles. *Appl. Catal. B* **2017**, *202*, 683–694. [CrossRef]

53. Luisetto, I.; Tuti, S.; Di Bartolomeo, E. Co and Ni supported on CeO$_2$ as selective bimetallic catalyst for dry reforming of methane. *Int. J. Hydrog. Energy* **2012**, *37*, 15992–15999. [CrossRef]

54. Rotaru, C.G.; Postole, G.; Florea, M.; Matei-Rutkovska, F.; Parvulescu, V.I.; Gelin, P. Dry reforming of methane on ceria prepared by modified precipitation route. *Appl. Catal. A Gen.* **2015**, *494*, 29–40. [CrossRef]

55. Laosiripojana, N.; Assabumrungrat, S. Catalytic dry reforming of methane over high surface area ceria. *Appl. Catal. B Environ.* **2005**, *60*, 107–116. [CrossRef]

56. Yap, D.; Tatibouët, J.-M.; Batiot-Dupeyrat, C. Catalyst assisted by non-thermal plasma in dry reforming of methane at low temperature. *Catal. Today* **2018**, *299*, 263–271. [CrossRef]

57. Signoretto, M.; Menegazzo, F.; Di Michele, A.; Fioriniello, E. Effects of Support and Synthetic Procedure for Sol-Immobilized Au Nanoparticles. *Catalysts* **2016**, *6*, 87. [CrossRef]

58. Tang, M.; Liu, K.; Roddick, M.D.; Fan, M. Enhanced lattice oxygen reactivity over Fe2O3/Al2O3 redox catalyst for chemical-looping dry (CO$_2$) reforming of CH4: Synergistic La-Ce effect. *J. Catal.* **2018**, *368*, 38–52. [CrossRef]

59. Yang, R.; Xing, C.; Lv, C.; Shi, L.; Tsubaki, N. Promoting effect of La$_2$O$_3$ and CeO$_2$ on Ni/γ-Al$_2$O$_3$ catalysts for CO$_2$ reforming of CH4. *Appl. Catal. A Gen.* **2010**, *385*, 92–100. [CrossRef]

60. Charisiou, N.D.; Siakavelas, G.; Papageridis, K.N.; Baklavaridis, A.; Tzounis, L.; Avraam, D.G.; Goula, M.A. Syngas Production via the biogas dry reforming reaction over nickel supported on modified with CeO_2 and/or La_2O_3 alumina catalysts. *J. Nat. Gas Sci. Eng.* **2016**, *31*, 164–183. [CrossRef]

61. Pino, L.; Vita, A.; Cipitì, F.; Laganà, M.; Recupero, V. Hydrogen production by methane tri-reforming process over Ni–ceria catalysts: Effect of La-doping. *Appl. Catal. B* **2011**, *104*, 64–73. [CrossRef]

62. Pizzolitto, C.; Menegazzo, F.; Ghedini, E.; Innocenti, G.; Di Michele, A.; Cruciani, G.; Cavani, F.; Signoretto, M. Increase of Ceria Redox Ability by Lanthanum Addition on Ni Based Catalysts for Hydrogen Production. *ACS Sustain. Chem. Eng.* **2018**. [CrossRef]

63. Kundakovic, L.; Flytzani-Stephanopoulos, M. Cu- and Ag-Modified Cerium Oxide Catalysts for Methane Oxidation. *J. Catal.* **1998**, *179*, 203–221. [CrossRef]

64. Gregg, S.J.; Sing, K.S.W. *Adsorption, Surface Area and Porosity*, 2nd ed.; Academic Press: Cambridge, MA, USA, 1982; p. 111.

65. Dong, W.; Roh, H.; Jun, K.; Park, S.; Oh, Y. Methane reforming over Ni/Ce-ZrO$_2$ catalysts: Effect of nickel content. *Appl. Catal. A* **2002**, *226*, 63–72. [CrossRef]

66. Gould, T.D.; Izar, A.; Weimer, A.; WFalconer, J.L.; Medlin, J.W. Stabilizing Ni Catalysts by Molecular Layer Deposition for Harsh, Dry Reforming Conditions. *ACS Catal.* **2014**, *4*, 2714–2717. [CrossRef]

67. Xie, X.; Otremba, T.; Littlewood, P.; Schomäcker, R.; Thomas, A. One-Pot Synthesis of Supported, Nanocrystalline Nickel Manganese Oxide for Dry Reforming of Methane. *ACS Catal.* **2013**, *3*, 224–229. [CrossRef]

68. Wang, L.; Liu, H.; Liu, Y.; Chen, Y.; Yang, S. Influence of preparation method on performance of Ni-CeO$_2$ catalysts for reverse water-gas shift reaction. *J. Rare Earths* **2013**, *31*, 559–564. [CrossRef]

69. Biswas, P.; Kunzru, D. Steam reforming of ethanol for production of hydrogen over Ni/CeO$_2$–ZrO$_2$ catalyst: Effect of support and metal loading. *Int. J. Hydrog. Energy* **2007**, *32*, 969–980. [CrossRef]

70. Gonzalez-DelaCruz, V.M.; Holgado, J.P.; Perenìguez, R.; Caballero, A. Morphology changes induced by strong metal–support interaction on a Ni–ceria catalytic system. *J. Catal.* **2008**, *257*, 307–314. [CrossRef]

71. Marrero-Jerez, J.; Larrondo, S.; Rodríguez-Castellón, E.; Núñez, P. TPR, XRD and XPS characterisation of ceria-based materials synthesized by freeze-drying precursor method. *Ceram. Int.* **2014**, *40*, 6807–6814. [CrossRef]

72. Mandapaka, R.; Madras, G. Aluminium and rhodium co-doped ceria for water gas shift reaction and CO oxidation. *Mol. Catal.* **2018**, *451*, 4–12. [CrossRef]

73. Glass, D.E.; Galvan, V.; Prakash, G.K.S. The Effect of Annealing Temperature on Nickel on Reduced Graphene Oxide Catalysts on Urea. Electrooxidation. *Electrochim. Acta* **2017**, *253*, 489–497. [CrossRef]

74. Keating, P.R.L.; Scanlon, D.O.; Watson, G.W. The nature of oxygen states on the surfaces of CeO$_2$ and La-doped CeO$_2$. *Chem. Phys. Lett.* **2014**, *608*, 239–243. [CrossRef]

75. Shen, W.; Momoi, H.; Komatsubara, K.; Saito, T.; Yoshida, A.; Naito, S. Marked role of mesopores for the prevention of sintering and carbon deposition in dry reforming of methane over ordered mesoporous Ni–Mg–Al oxides. *Catal. Today* **2011**, *171*, 150–155. [CrossRef]